Met. Mater. Int., Vol. 21, No. 4 (2015), pp. 746~752
doi: 10.1007/s12540-015-5012-7

Effect of Pressing Routes on the Microstructure and Strength in Equal Channel Angular Pressing of Cu-3.75Ag

Fahamsyah Hamdan Latief[1,2] and Sun Ig Hong[1,*]

[1]Department of Nanomaterials Engineering, Chungnam National University, Taedok Science Town, Daejon 305-764, Korea
[2]Department of Mechanical Engineering, Al Imam Mohammad Ibn Saud Islamic University, Riyadh 11432, Kingdom Saudi Arabia

(received date: 6 January 2015 / accepted date: 17 February 2015)

The combined effects of thermo-mechanical treatment and equal channel angular pressing (ECAP) on the strength and microstructure of Cu-3.75Ag were studied. The strength of Cu-3.75Ag at 1% strain after eight passes of ECAP with two intermediate heat treatments reached 758 MPa and 849 MPa in route A and route Bc respectively. The hardness increased upon heat-treatment in route Bc, in contrast to the drop of the hardness in route A, suggesting that the hardening caused by re-precipitation is more active due to more effective dissolution of second-phase particles in route Bc. The flow stress increased more rapidly with intermediate heat treatments and reached 842 MPa after 8 passes, greater than that (791 MPa) without intermeadiate heat treatment in route Bc. The more rapid increase of strength/hardness and the attainment of higher hardness/strength after intermediate heat treatment are likely to be attributed to the formation of more stable wall structure and rearrangement of solute atoms/precipitates. The spacing between precipitates in Cu-3.75Ag ECAPed for 4 pass in route Bc was measured to be approximately 12.5 nm, which is close to the calculated activated length (12.8 nm). The most probable rate controlling mechanism of Cu-3.75 Ag is suggested to be the interaction between dislocations and precipitates.

Keywords: severe plastic deformation, mechanical properties, strength, microstructure, activation analysis

1. INTRODUCTION

Equal-channel angular pressing (ECAP) of alloys and composites have attracted more interests because it rendered the promising physical and mechanical properties without any significant reduction of the cross-sectional area of the alloys and composites unlike the other severe deformation processing such as rolling, extrusion and drawing [1-14]. Recently Cho and Hong [2] employed ECAP processing to refine the two-phase structure of Cu-15 wt% Ag composites and obtained the good strength-conductivity properties. They [2] observed that ECAPed Cu-15 wt% Ag composite exhibited ultrafine two-phase structure with the shape and distribution of Ag phase dependent on the processing routes. The Ag filaments with the thickness of 3-5 nm and the elongated subgrains with the width of 45-70 nm were observed in ECAPed Cu-15 wt% Ag [2].

Cu-Ag composites with high silver content (>15 wt%) possess three to four times the strength of cold-worked copper, while maintaining high conductivity (>80% IACS). Both the mechanical and electrical properties of these composites depend upon the composition, degree of cold work, and intermediate heat treatments [8,9]. The general application and use of Cu-Ag composites and alloys with high silver contents are limited by the high cost of the material. The needs for Cu-Ag alloys with excellent strength/conductivity properties, but with lower Ag contents are growing because of the high silver price. The mechanical and electrical properties of the Cu-Ag alloy with lower silver content can be improved by the optimization of thermo-mechanical processing [2,9-11].

In this study, effect of ECAP processing on the microstructure and mechanical properties of the Cu-3.75Ag were investigated. The present study has been carried out to examine the possible ways to improve the mechanical properties of Cu-Ag alloys with lower silver content by thermo-mechanical ECAP processing. The mechanical and microstructural stability of Cu-3.75Ag alloy were examined and correlated with the microstructural change caused by thermo-mechanical treatments.

2. EXPERIMENTAL PROCEDURE

Cu-3.75Ag (in wt%) alloy used in this study was prepared by an induction melting in vacuum. Prior to ECAP, the ingots were homogenized at 850 °C for 24 h and subsequently water-

*Corresponding author: sihong@cnu.ac.kr

quenched to achieve the homogenous distribution of second phase particles and alloying elements in the matrix. Rectangular-shaped rods with 5.5 mm×5.5 mm in cross section and 60 mm in length were machined for ECAP processing. The die used for ECAP consisted of two square channels with the cross section of 5.5 mm×5.5 mm intersecting at an angle of 90°, and the arc of curvature at the outer point of contact between channels was also 90°. Both die and the specimen were coated by molybdenum disulfide lubricant. In this research, two different of routes (A and Bc) were used for ECAP processing. The sample was pressed without rotation between each pass in route A, rotated by 90 degree after each pass in route Bc. All pressings were carried out at room temperature and at a speed of 5 mm/s. During the ECAP process, intermediate heat treatments (IHT) were employed to some specimen at 300 °C after four passes and 250 °C after six passes of ECAP for 2 h.

The mechanical properties were evaluated using compression tests at room temperature and a constant strain rate of 10^{-3} s^{-1}. The compression specimens with dimensions of 2 mm×2 mm in cross-section and 3 mm in length were cut parallel to the longitudinal axes of the ECAP direction. Strain rate jump test was also performed, from strain rate of 10^{-4} to 10^{-2} s^{-1}, at a strain of 10% in order to obtain the activation volume. The microstructures were characterized using transmission electron microscope (TEM).

3. RESULTS AND DISCUSSION

3.1. Variation of hardness and strength

The Vickers microhardness, Hv, is plotted in Fig. 1(a) and 1(b) as a function of number of ECAP passes with or without intermediate heat treatment (IHT) using route A (a) and Bc (b). The sample was pressed without rotation between each pass in route A, rotated by 90 degree after each pass in route Bc. The hardness of Cu-3.75Ag using route A increased significantly after one pass of ECAP. The micro-Vickers hardness was found to increase gradually with the number of ECAP passes without intermediate heat treatment as shown in Fig. 1(a). With intermediate heat treatments, the hardness dropped slightly after intermediate heat treatment and recovered rapidly with further pressing by route A. A slight decrease of the hardness by annealing at 300 °C after 4 passes and 250 °C after 6 passes indicates that the softening occurred primarily due to recovery during intermediate heat treatment in route A. The hardness, however, increased more rapidly with intermediate heat treatments and reached 241 Hv after 8 passes, greater than that (220 Hv) without intermeadiate heat treatment in route A. Hong and Hill [11] suggested that the morphological modification and redistribution of second phase during IHT increased the hardening rate with ECAP passes after IHT.

In Fig. 1(b), the hardness increases gradually, but more rapidly with number of passes in route Bc than in route A for both conditions, without and with intermediate heat treatments

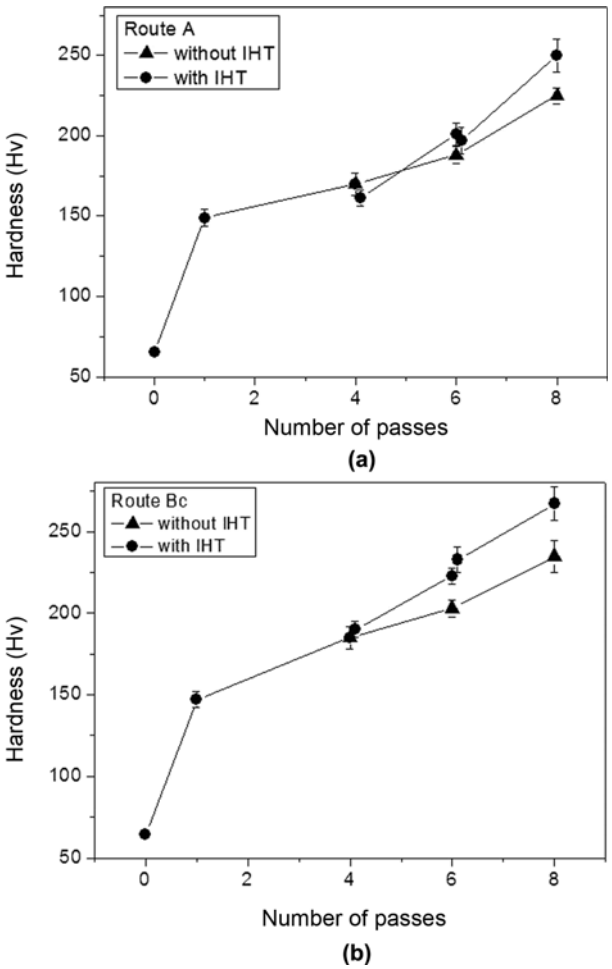

Fig. 1. The hardness of ECAPed Cu-3.75Ag as a function of number of passes; (a) route A and (b) route Bc.

(IHT). The hardness also increased more rapidly with intermediate heat treatments and reached 261 Hv after 8 passes, greater than that (242 Hv) without intermeadiate heat treatment in route Bc. One interesting observation is that the hardness increased just after intermediate heat treatment after 4 passes and 6 passes in route Bc, in contrast to the drop of the hardness just after heat treatment in route A (Fig. 1(a)).

The variation of compressive flow stress at 1% strain of Cu-3.75Ag is plotted in Fig. 2(a) and 2(b) as a function of number of ECAP passes with or without intermediate heat treatment (IHT) using route A (a) and Bc(b). The strength of as-homogenized sample is 104 MPa at 1% strain. The strength of Cu-3.75Ag increased significantly to 492 MPa just after application of one pass of ECAP. The strength continued to increase gradually to 780MPa after 8 passes without intermediate heat treatment using route A as shown in Fig. 2(a). With intermediate heat treatments, the flow stress dropped after intermediate heat treatment and recovered rapidly with further pressing in route A as in hardness measurements. The slight decrease of the flow stress by annealing at 300 °C

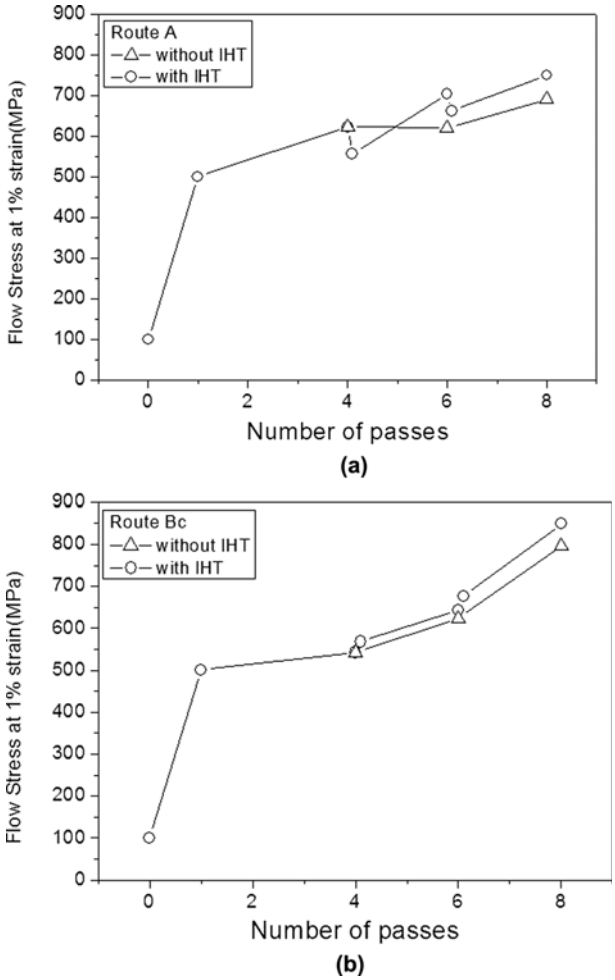

Fig. 2. The flow stress of ECAPed Cu-3.75Ag at 1% strain as a function of number of passes; (a) route A and (b) route Bc.

after 4 passes and 250 °C after 6 passes supports the softening of the cold-worked matrix due to recovery during intermediate heat treatment in route A. It is interesting to note that the flow stress again increased more rapidly with intermediate heat treatments and reached 758 MPa after 8 passes, greater than that (691MPa) without intermeadiate heat treatment in route A. The rapid increase of the flow stress after IHT can be mostly attributed to the morphological modification and redistribution of second phase particles during recovery [1,2,11,15].

In Fig. 2(b), the flow stress also increased more rapidly with intermediate heat treatments and reached 849 MPa after 8 passes, greater than that (791 MPa) without intermeadiate heat treatment in route Bc. The flow stress also increased just after intermediate heat treatment after 4 passes and 6 passes in route Bc, in contrast to the observation in route A (Fig. 1(a)), suggesting the enhanced contribution of alloying elements and/or precipitates is greater in route Bc than in route A. The cold-worked dislocation structure in the absence of effects of alloying and second phase particles is subject to recovery by heat-treatment at intermediate temperatures, resulting in softening. The increase of hardness with heat treatment in Bc processing suggests that the redistribution of solute atoms such as re-precipitation is more prevalent and active due to the more effective dissolution of second phase particles during ECAP processing by route Bc [2,15].

3.2. Microstructural evolution

Cho and Hong and Choi *et al*. [15] observed in Cu-15 wt% Ag microcomposite and Cu-Fe based microcomposites that the second phase lamellae and dendrites developed into elongated filamentary structure due to the accumulative strain toward the same pressing direction in route A. On the other hand, sheared and fragmented second phase particles were formed due to shearing of the matrix and the second phase in multiple directions caused by the sample rotation by 90 degrees after each pass in route Bc. The population of Ag or Fe particles, therefore, was observed to increase significantly by ECAP processing using route Bc. In Cu-3.75 wt% Ag alloy of the present study, small precipitates are likely to be sheared and dissolved more frequently in route Bc due to the activation of multiple slip systems than in route A, which would precipitate and strengthen the matrix during heat treatment at intermediate temperatures. Choi *et al*. [15] also observed more frequent shearing and gradual dissolution of Fe dendrites and particles in ECAPed Cu-Fe based microcomposites in Bc route. The enhanced dissolution of second phase particles by frequent fragmentation of particles in route Bc is likely caused by the dragging of solute atoms out from particles by passing dislocations on multiple slip planes and the instability of small sheared particles due to the increase of surface energy. Second phase particle dissolution and enhanced solubility of alloying elements in the matrix have been also reported in severely plastic-deformed Al alloys [16,17].

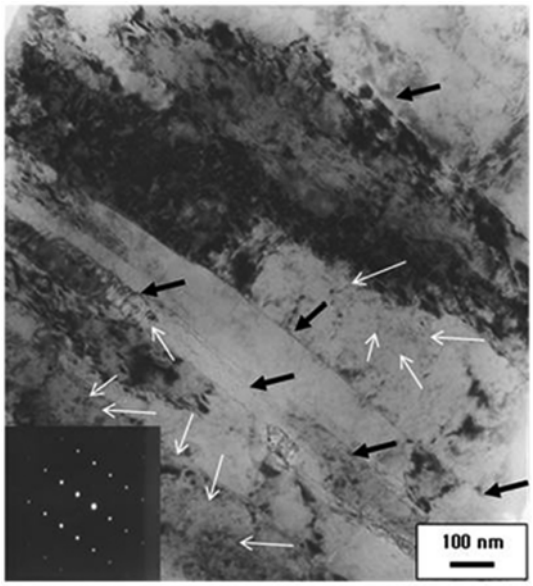

Fig. 3. TEM micrograph of Cu-3.75Ag after one pass of ECAP.

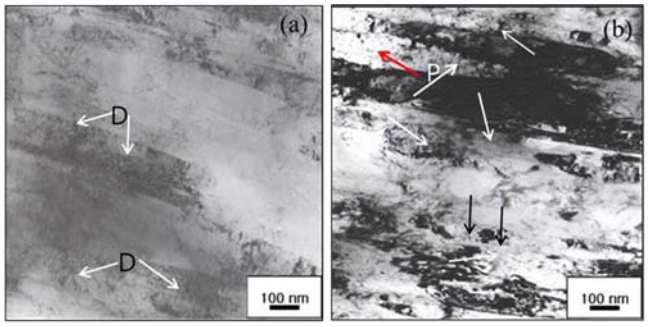

Fig. 4. TEM micrographs of Cu-3.75Ag after four passes of ECAP by route A : (a) without and (b) with one intermediate heat treatment.

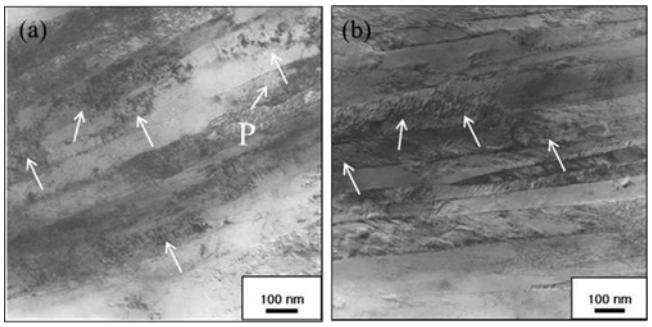

Fig. 5. TEM micrographs of Cu-3.75Ag after four passes of ECAP by route Bc : (a) without and (b) with one intermediate heat treatment.

TEM micrograph after one pass of ECAP is shown in Fig. 3, together with SAED patterns. Examination of the TEM microstructure revealed that the dense dislocation walls and/or elongated cell walls (indicated by black arrows) parallel to the primary slip plane with array of dislocations spanning these walls. The presence of small Ag precipitates/particles (indicated by white arrows) should also be noted. The width between dislocation/cell walls was observed to be 219±28 nm.

TEM microstructures of Cu-3.75Ag after 4 passes of ECAP without (a) and with (b) one heat treatment using route A are shown in Fig. 4(a). The microstructure features are still dominated by elongated cell and dislocation walls between which some loosely-knit dislocations and array of dislocations (marked with "D") are visible. Because of the strain field of numerous dislocations between the cell/dislocation walls, the image of dislocations appear to be indistinct. The width between dislocation/cell walls decreased to 142±21 nm. After first intermediate heat treatment, the population of dislocations between walls decreased as evidenced by the clear images of the matrix between walls in Fig. 4(b). Ag precipitates (indicated by arrows) were also clearly visible after one intermediate heat treatment. The wall boundary also appeared to be clearer, as supported by the more drastic change of the contrast. The width between wall boundaries increased slightly to 150±18 nm.

TEM microstructures of Cu-3.75Ag after 4 passes of ECAP without (a) and with (b) one heat treatment using route Bc are shown in Fig. 5. The microstructure features are still dominated by elongated cell and dislocation walls between which some loosely-knit dislocation tangles are visible. The general microstructural features are not much different from that shown in Fig. 4(a). The width between dislocation/cell walls was observed to be 138±16 nm. After first intermediate heat treatment, the dislocations between walls appeared to be rearranged to reach the energetically stable structure [15-18] as evidenced by the much clearer images of the matrix in Fig. 5(b) because of dislocation rearrangement and annihilation. The precipitates are indicated by arrows in Fig. 5.

The wall boundary after heat treatment also became much sharper, suggesting the dislocations in the boundary also rearranged to reach the lower energy state. The width between wall boundaries was observed to be 134±15 nm. Dislocation wall and cell boundaries are typical forms of low energy dislocation structure [18-21]. During room temperatures ECAP processing, dislocations are generated and arranged to reach the dislocation structure with a lower energy. However, solute atoms, precipitates and other dislocations can be obstacles to the rearrangement of dislocations [18-22] toward the lower energy dislocation structure, which requires thermal activations. As shown in Fig. 3, Fig. 4(a) and Fig. 5(a), numerous dislocation arrays and loosely-knit dislocation tangles were observed between the dislocation/cell walls just after ECAP processing at room temperature. Dislocations between dislocation/cell walls and those in walls tend to rearrange themselves to lower the strain energy of dislocations during heat treatment and are likely to annihilate each other and/or deposit on the walls during heat treatment to lower the strain energy [18-21], reducing the dislocation density in Cu channels between walls as shown in Fig. 4(b) and 5(b). Dislocations in dislocation/cell walls also rearrange themselves and, therefore, the boundary became much clearer and sharper because of the locally increased misorientation across the thinner boundary [18-21]. Therefore, the dislocations/cell walls became more closely-knit structure during heat treatment and could act as more stable obstacles to dislocation motion. The more rapid increase of strength/hardness and the attainment of higher hardness/strength after heat treatment at intermediate temperatures are likely to be attributed to the formation of more stable wall structure and rearrangement of solute atoms/precipitates.

Figures 6(a) and 6(b) exhibit TEM microstructures of Cu-3.75Ag after six passes of ECAP without (a) and with (b) two intermediate heat treatments using route A. After 6 ECAP passes without IHT, more dislocations were observed in Cu matrix between dislocation/cell boundary and the spacing between the walls decreased to 122±13 nm. After 6 passes with two IHT in route A, the spacing (130±17 nm) between dislocation/cell walls slightly larger than that without IHT and the population of dislocation in the Cu matrix between walls appeared to be decreased. It should be noted that the

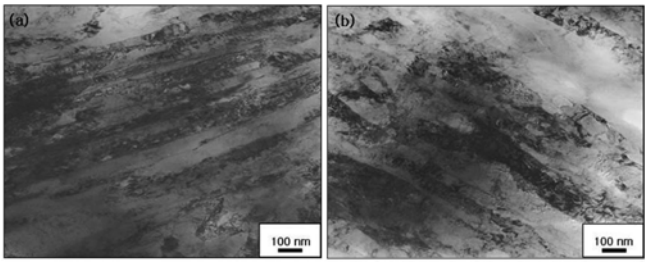

Fig. 6. TEM micrographs of Cu-3.75Ag after six passes of ECAP by route A : (a) without and (b) with two intermediate heat treatment.

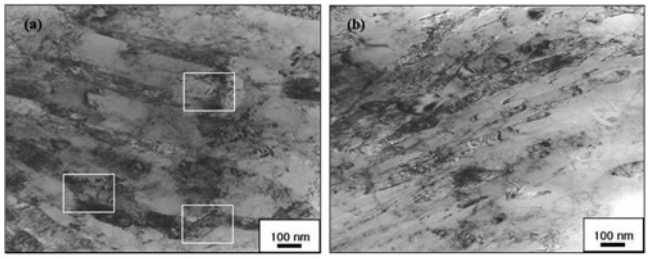

Fig. 7. TEM micrographs of Cu-3.75Ag after six passes of ECAP by route Bc : (a) without and (b) with two intermediate heat treatment.

dislocation wall boundaries are mostly parallel to the one primary direction, suggesting that these walls were formed on the primary slip planes.

Figures 7(a) and 7(b) exhibit TEM microstructures of Cu-3.75Ag after six passes of ECAP without (a) and with (b) two intermediate heat treatments using route Bc. In route Bc after 6 ECAP passes without IHT, the spacing between dislocation/cell boundary walls was observed to be 124±18 nm, close to that of route A. But, the microstructural features appear to be a little complicated. For example, some short intersecting cell walls (marked with rectangles) were observed at the inclined angle to the primary slip directions. It should be noted that the spacing (117±13 nm) between wall boundaries after 6 ECAP passes with two IHT in Fig. 7(b) was found to be smaller than that (124±18 nm) after 6 passes without two IHTs. After two IHT, wall boundaries became much clearer. In general, the spacing between wall boundaries decreased and the misorientation across the wall boundary increased with deformation strain [18]. Hansen and Kuhlmann-Wilsdorf [18] reported that the spacing between dense dislocation walls was ~200 nm at the strain of 1 and ~100 nm at the strain of 2 in Ni. The spacing in Cu-3.75Ag in this study was observed to be 219±28 nm after 1 pass (equivalent to the strain of ~1) and ~120 nm after 4 passes (equivalent to the strain of ~4), close to those in Ni. The misorintation angle across the wall boundary was reported to be 5° at the strain of 1 and 17° at the strain of 4 in Ni [18]. The spacing between dense dislocation/cell walls steadily decreased with number of ECAP passes for both with intermediate heat treatments and non-intermediate heat treatment regardless of heat pressing conditions (route A and route Bc).

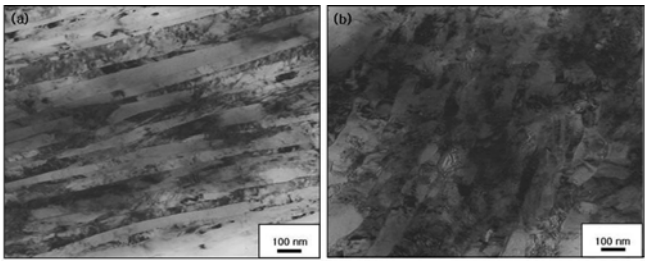

Fig. 8. TEM micrographs of Cu-3.75Ag after eight passes of ECAP with two intermediate heat treatments using (a) route A and (b) route Bc.

Figures 8(a) and 8(b) exhibit TEM microstructures of Cu-3.75Ag after eight passes of ECAP with two intermediate heat treatments using A (a) and Bc (b) routes. In Route A, well developed dense dislocation wall structures were observed. The spacing between the walls decreased to 121±12 nm after 8 ECAP passes with 2 IHTs. In the ECAPed sample for 8 passes with two heat treatments using route Bc, the dense dislocation walls and elongated subgrains were well developed and spacing between walls decreased to 115±11 nm. It should be noted that rather short cell/subgrain walls were also well developed intersecting the long dislocation walls, compatible with the multiple slip activities due to 90 degree rotation after each pass. The wall boundary became sharper and the alternating sense of contrast across the walls suggests that the misorientation angle across the boundary increased after two IHTs in both route A and route Bc.

3.3. Activation volume and strengthening mechanism

In order to investigate the rate controlling mechanism for deformation of Cu-3.75Ag, strain rate change tests were performed and the activation volumes for plastic flow were measured. The activation volume associated with the deformation process has been obtained from the following classical equation [23]:

$$V^* = kT\,\partial \ln\dot{\gamma}/\partial\tau = mkT\,(\ln\dot{\varepsilon}_2 - \ln\dot{\varepsilon}_1)/(\tau_2-\tau_1) \quad (1)$$

where k is the Boltzmann's constant, $\dot{\gamma}$ the shear strain rate, τ the shear stress, s_1 and s_2 the applied shear stresses at the normal strain rates $\dot{\varepsilon}_1$ and $\dot{\varepsilon}_2$, respectively and T is the absolute temperature. The shear stress τ was calculated from the yield stress σ using the relation $\tau = \sigma/m$, where m is the Taylor factor. The calculated apparent activation volume was 68.5 b3 (where b is the burgers vector for Cu (=0.256 nm)) for as-cast Cu-3.75Ag at room temperature. The calculated activation volume was summarized in Table 1.

The activation volume gradually decreased with increase of number of ECAP passes in both route A and route Bc. The activation volumes of the ECAPed specimen for 8 passes without intermediate heat treatment were 33.1 b^3 and 25.6 b^3 for route A and route Bc, respectively. It is noted that the activation volume in route Bc is smaller than in route A, sug-

Table 1. Activation volumes of Cu-3.75Ag before and after ECAP

Processing	Condition	Activation volume	
As-cast	initial	$68.5b^3$	
	Number of pass	Route A	Route Bc
ECAP (no heat treatment)	1	$52.7\ b^3$	$52.7\ b^3$
	4	$54.3\ b^3$	$50.3\ b^3$
	6	$47.9\ b^3$	$36.8\ b^3$
	8	$33.1\ b^3$	$25.6\ b^3$
ECAP (with heat treatment)	4 (1 HT)	$49.3\ b^3$	$44.5\ b^3$
	6 (2 HT)	$35.9\ b^3$	$29.2\ b^3$
	8 (2 HT)	$31.4\ b^3$	$20.4\ b^3$

gesting that the spacing of obstacles for thermally activated deformation is smaller in route Bc. The activation volumes of the ECAPed specimen for 8 passes with 2 intermediate heat treatments(IHT) was 31.4 b^3 and 20.4 b^3 for route A and route Bc, respectively. Again, the activation volume in route Bc was smaller in the ECAPed specimen with two IHT. It is interesting to note that the activation volume of the ECAPed specimen for 8 passes with two IHT is smaller than that without IHT, suggesting that the spacing of obstacles for thermally activated deformation decreased in the specimen with intermediate treatments.

The decrease of the activation volume with number of ECAP pass can be attributed to the increase of dislocation density and the redistribution and re-precipitation of second phase particles, which was reported to be re-precipitated at low temperatures after heavy deformation [23]. The activation volume measured in this study is smaller than that (150~170 b^3) of Cu-9 Fe-1.2 Ag by Song *et al*. [23]. The smaller activation volume observed in this study is likely to be associated with higher Ag content in this study. Ag precipitates are more likely to be redistributed during deformation and heat treatment cycles because of its lower shearing strength. The spacing between obstacles for the thermally activated deformation of Cu-3.75Ag after 8 ECAP passes from the activation volume data in Table 1 is 20~70b (=5~18 nm). The activated length (=5~18 nm) measured in this study was much smaller than the spacing (110-170 nm) between dense dislocation walls, suggesting they are not the rate-controlling obstacles for the thermally activated deformation. Hong and Hill [11] observed numerous second phase particles in Cu-Ag nanocomposites and small second-phase particles in Cu matrix were suggested to result from reprecipitation of the second phase that had dissolved during heavy deformation processing. It was suggested recently that the most probable rate controlling mechanism of Cu-Fe-Ag [23] and Cu-Fe-Cr [24] microcomposites was the interaction between dislocations and precipitates in Cu matrix.

The spacing between precipitates in Cu-3.75Ag ECAPed for 1 pass was measured to be approximately 15.1 nm from TEM microstructure (Fig. 1), which is close to the calculated activated length (13.5 nm). The spacing between precipitates in Cu-3.75Ag ECAPed for 4 pass in route Bc (Fig. 5(a)) was measured to be approximately 12.5 nm from Fig. 5(a), which is close to the calculated activated length (12.8 nm). For the ECAPed specimens with higher ECAP passes (>6), the spacing between Ag precipitates cannot be measured accurately because of the increased dislocation density and the narrower spacing between dense dislocation walls. Small second-phase particles in Cu matrix were suggested to result from reprecipitation of the second phase that had dissolved during heavy deformation processing, resulting in the finer redistribution of precipitates.

Hong and coworkers [11,25] suggested that the filaments, elongated sub-grain, grain boundaries and dense dislocation walls in Cu base microcomposites are athermal obstacles and contribute to the athermal strengthening component. In Cu base microcomposites, the ratio of yield stresses was found to be 0.92, which is close to that of Young's moduli (0.91) [11,25]. The dense dislocation walls/subgrain boundaries with the spacing of 110~170 nm in Cu-3.75Ag of the present study are not likely the rate controlling obstacles during plastic deformation. They are athermal obstacles which increase the strength by increasing the long-range internal stress and less likely to be strain rate sensitive despite its significant contribution to the strength.

4. CONCLUSIONS

Based upon a study on the microstructure and strength of Cu-3.75Ag, the following conclusions can be drawn:

(1) The flow stress increased more rapidly with intermediate heat treatments and reached 842 MPa after 8 passes, greater than that (791 MPa) without intermeadiate heat treatment in route Bc. In route A, the flow stress reached 758 MPa after 8 passes with intermediate heat treatments and, greater than that (691MPa) without intermeadiate heat treatment.

(2) The hardness increased just after intermediate heat treatment after 4 passes and 6 passes in route Bc, in contrast to the drop of the hardness just after heat treatment in route A. The increase of hardness with heat treatment in Bc processing suggests that the redistribution of solute atoms such as re-precipitation is more prevalent and active due to the more effective dissolution of second phase particles during ECAP processing by route Bc.

(3) The more rapid increase of strength/hardness and the attainment of higher hardness/strength after intermediate heat treatment (IHT) are likely to be attributed to the formation of more stable wall structure and rearrangement of solute atoms/precipitates.

(4) The spacing between precipitates in Cu-3.75Ag ECAPed for 4 pass in route Bc was measured to be approximately 12.5 nm, which is close to the calculated activated length (12.8 nm). The most probable rate controlling mechanism of Cu-3.75 Ag is suggested to be the interaction between dislocations and

precipitates.

(5) In Route A and Bc, well developed dense dislocation wall structures were observed after 8 passes with two IHT and the spacing between the dense dislocation walls was observed to be 121±12 nm and 115±11 nm respectively.

ACKNOWLEDGEMENT

This work was supported by the 2nd phase of the Fundamental R&D Programs for Core Technology of Materials funded by Ministry of Trade, Industry and Energy (2014-2015).

REFERENCES

1. R. Z. Valiev, A. V. Korznikov, and R. R. Mulyukov, *Mater. Sci. Eng. A* **A168**, 141 (1993).
2. K.-J. Cho and S. I. Hong, *Met. Mater. Int.* **18**, 355 (2012).
3. I. H. Lee, S. I. Hong, and K. H. Lee, *Korean J. Met. Mater.* **50**, 931 (2012).
4. H. S. Kim, S.-H. Joo, and H. J. Jeong, *Korean J. Met. Mater.* **52**, 87 (2014).
5. M. Vaseghi, A. K. Taheri, and H. S. Kim, *Met. Mater. Int.* **16**, 363 (2010).
6. W. J. Kim, C. S. Chung, D. S. Ma, S. I. Hong, and H. K. Kim, *Scripta Mater.* **49**, 333 (2003).
7. K.T. Park, D. Y. Hwang, and D. H. Shin, *Met. Mater. Int.* **8**, 519 (2002).
8. Y. Iwahashi, Z. Horita, M. Nemoto, and T. G. Langdon, *Acta mater.* **45**, 4733 (1997).
9. S. I. Hong, M. A. Hill, Y. Sakai, J. T. Wood, and J. D. Embury, *Acta Metall. Mater.* **43**, 3313 (1995).
10. M. S. Lim, J. S. Song, and S. I. Hong, *J. Mater. Sci.* **35**, 4557 (2000).
11. S. I. Hong and M. A. Hill, *Acta Metall. Mater.* **46**, 4111 (1998).
12. M. Seyed Salehi, N. Anjabin, and H. S. Kim, *Met. Mater. Int.* **20**, 825 (2014).
13. Y. Song, W. Wang, D. J. Lee, H. J. Jeong, S.H. Lee, and H. S. Kim, *Met. Mater. Int.* **21**, 7 (2015).
14. K. H. Lee and S. I. Hong, *Korean J. Met. Mater.* **51**, 621 (2013).
15. Y. C. Choi, H. S. Kim, and S. I. Hong, *Met. Mater. Int.* **15**, 733 (2009).
16. G. Angella, P. Bassani, A. Tuissi, and M. Vedani, *Mater. Trans.* **45**, 2182 (2004).
17. S. I. Hong, G. T. Gray III, and J. J. Lewandowski, *Acta Metal. Mater.* **41**, 2337 (1993).
18. N. Hansen and D. Kuhlmann-Wilsdorf, *Mater. Sci. Eng.* **81**, 141 (1986).
19. S. I. Hong and C Laird. *Acta Metal. Mater.* **38**, 1581 (1990).
20. D. Kuhlmann-Wilsdorf, *Mater. Sci. Eng.* **86**, 53 (1987).
21. D. Kuhlmann-Wilsdorf, *Mater. Sci. Eng.* **315**, 211 (2001).
22. J. S. Ha and S. I. Hong, *Mater. Mater. Sci. Eng. A* **A565**, 9 (2013).
23. J. S. Song, S. I. Hong, and Y. G. Park, *J. Alloy. Comp.* **388**, 69 (2005).
24. Y. S. Kim, J. S. Song, and S. I. Hong, *J. Mater. Proc. Technol.* **130**, 278 (2002).
25. S. I. Hong, *Adv. Eng. Mater.* **3**, 475 (2001).